Lessons learnt from OECD/NEA Phase II-C through Phase II-E Benchmarks

Jens Christian Neuber
AREVA NP GmbH, Department NEEA-G, Offenbach, Germany
jens-christian.neuber@areva.com

Abstract

It is demonstrated that the knowledge gained from the OECD/NEA Phases II-C through II-E helps to understand and to predict qualitatively the reactivity behavior of spent PWR UO_2 fuel assembly configurations and to avoid, therefore, errors in the design of devices, systems or installations for handling, transport or storage of spent PWR UO_2 fuel assemblies.

1 Introduction

The main objective of the Phase II of the OECD/NEA benchmark program was to study the impact of axial burnup profiles on the reactivity of spent PWR UO_2 fuel assembly configurations. Whereas simplified model burnup profiles were used in Phase II-A and Phase II-B, since the benchmarks of these phases were addressed to basic studies (cf. [1] and [2]), and whereas a uniform burnup profile was actually used in Phase II-D, because in this phase the attention was focused on the effect of control rod insertion during irradiation of PWR UO_2 fuel assemblies on the spent fuel composition, realistic axial burnup profiles extracted from databases of real axial burnup profiles were used in Phase II-C and Phase II-E. The attention is mainly focused on these two phases in the following and on lessons that can be learnt from the results obtained for the benchmark configurations used in these phases.

1.1 Objective of the Phase II-C benchmark and summary of results of this benchmark

The objective of Phase II-C was to study the impact of the asymmetry of axial burnup profiles of spent PWR UO_2 fuel assemblies on the end effect, cf. [3]. The end effect related to a given axial burnup profile expresses the impact of this profile on the reactivity of a given spent PWR UO_2 fuel assembly configuration and is defined as the difference of the configuration's neutron multiplication factor $k_{eff}(\text{shape})$ obtained by using the actual shape of the profile and the configuration's neutron multiplication factor $k_{eff}(\text{unif. dist.})$ obtained by using the uniform distribution of the averaged burnup of the profile,

$$\text{end effect} \equiv \Delta k_{ee} = k_{eff}(\text{shape}) - k_{eff}(\text{unif.dist.}) \qquad (1)$$

As will be described in more detail in section 2.2, the following observations were made in Phase II-C:

- The asymmetry of axial burnup profiles tends to decrease with increasing average burnup of the profiles.

- At given burnup the end effect increases with increasing asymmetry.
- At given asymmetry the end effect increases with increasing average burnup.
- The end effect is significantly impacted by the "local asymmetry" of the profile in the region of the top end of the fuel zone of the fuel assemblies. This impact increases with increasing burnup.

1.2 Objective of the Phase II-D benchmark and summary of results of this benchmark

In Phase II-D the effect of control rod (CR) insertion during irradiation of PWR UO_2 fuel assemblies on the spent fuel composition was studied, cf. [4]. It was found that, due to spectrum hardening, CR insertion results in a change of the spent nuclear fuel (SNF) isotopic inventory; and it was demonstrated that, at given initial enrichment and given burnup, SNF which was exposed to CR insertion during irradiation has a higher reactivity than SNF which has not been exposed to CR insertion.

1.3 Objective of the Phase II-E benchmark

As already stated above, in Phase II-D the burnup was always assumed to be uniformly distributed over the active length of the fuel assemblies. Consequently, either zero CR insertion or full CR insertion (insertion over the full active length) were only assumed in Phase II-D. Therefore, it was the objective of Phase II-E benchmark to combine the asymmetry effect on the end effect with the CR insertion effect on the isotopic inventory as set forth below:

- Since the asymmetry of the axial profiles and the end effect are dependent on the average burnup of the profiles (cf. section 1.1) two profiles related to different average burnup values were chosen.
- To be representative and bounding the two axial burnup profiles chosen were generated from a database of real axial burnup profiles by means of the methods described in [5].
- For each of these profiles the end effect was studied for different CR insertion depths ranging from 0 cm (no insertion) to full insertion.

2 The Phase II-C benchmark

2.1 Brief description of the benchmark

The Phase II-C benchmark is based on the evaluation of a database of 850 axial burnup profiles, which has been provided by the German Convoy Series nuclear power plant Neckarwestheim II (cf. [6]). All the fuel assemblies from which these axial burnup profiles, based on evaluation of in-core flux map measurements, have been obtained are of one and the same type.

Since in an operating PWR core the temperature of the moderator increases during the passage of the moderator through the active zone from the bottom end to the top end of this zone the density

of the moderator decreases in this range (see Ref. [7] for example). Due to increasing spectrum hardening with decreasing moderator density an axial burnup profile is asymmetric in isotopic content and, in many cases, also in shape. Figure 1 shows typical examples from Ref. [6].

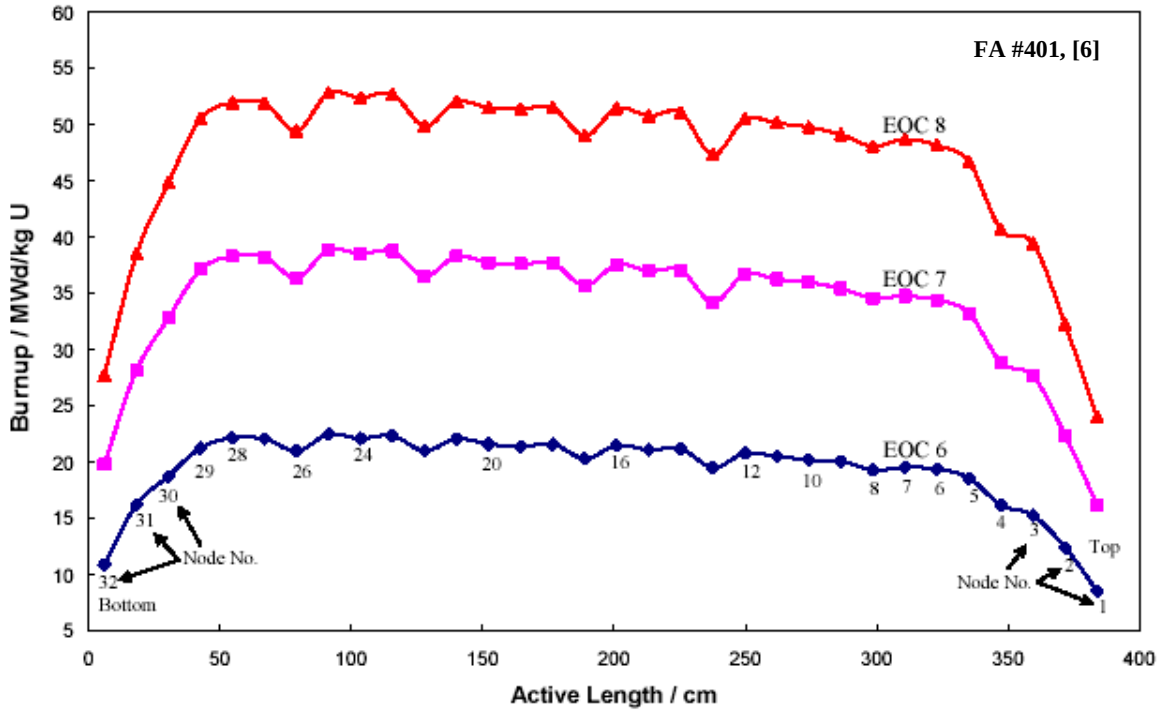

Figure 1*: Three typical PWR axial burnup profiles obtained for one and the same fuel assembly in three consecutive cycles [6]. These profiles are visibly asymmetric, and the positions of the spacer grids within the active zone are clearly seen.*
(Note that node no. 1 is the top node, i.e., node closest to the top end of the fuel zone, and node no. 32 is the bottom node, i.e., node closest to the bottom end of the active zone.)

The axial burnup profiles presented in Figure 1 are visibly asymmetric, and the positions of the spacer grids within the active zone are clearly seen (the presence of the spacer grids results in less moderation and hence less burnup in the range of these grids).

The asymmetry of axial burnup profiles is described by a parameter named as "top end parameter S6" [3] defined by eq. (2),

$$S\kappa(\mu) = \frac{1}{n}\sum_{\nu=1}^{\kappa} \alpha_{\nu\mu} \quad \text{with } \kappa = 6 \text{ and } n = 32\,, \tag{2}$$

where $\alpha_{\nu\mu}$ is the ratio of the burnup $B_{\nu\mu}$ of the μ-th profile at node ν to the averaged burnup $\overline{B}_{\mu}$ of this profile,

$$\alpha_{\nu\mu} = B_{\nu\mu} \big/ \overline{B}_{\mu}\,. \tag{3}$$

Since the nodes of the profiles from Ref. [6] are equidistant and since the distance of the bottom node to the bottom end of the active zone as well as the distance of the top node to the top end of the active zone are just given by the half of the distance between two neighboring nodes the averaged burnup $\overline{B}_\mu$ is given by eq. (4),

$$\overline{B}_\mu = \frac{1}{n}\sum_{\nu=1}^{n} B_{\nu\mu}\,,\ n = 32\,. \tag{4}$$

It follows, therefore,

$$\sum_{\nu=1}^{n=32} \alpha_{\nu\mu} = n = 32\,. \tag{5}$$

The 850 axial burnup profiles from Ref. [6] were normalized according to eq. (3) and grouped into seven groups according to their average burnup as specified in Figure 2. In this figure the average $\alpha_{\nu\mu}$ values of the normalized burnup profiles of each of the groups are presented. It appears from these group-averages $\alpha_{\nu\mu}$ that

- the asymmetry of axial burnup profiles tends to decrease with increasing average burnup of the profiles.

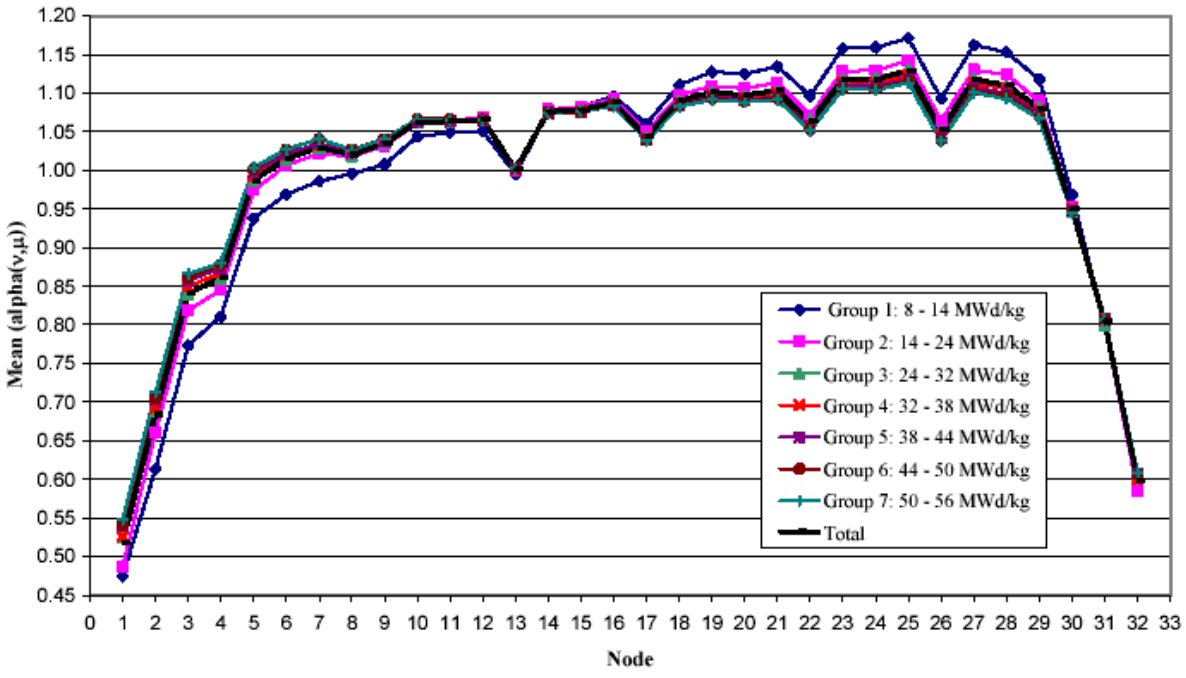

***Figure 2**: Evaluation of the axial burnup profiles from Ref. [6]: Averages $\alpha_{\nu\mu}$ for the burnup groups into which the normalized burnup profiles were grouped according to their average burnup values*

The choice of the top end parameter eq. (2) expresses the expectation that, due to the asymmetry of axial burnup profiles in the isotopic content, the neutron multiplication factor k_{eff} (shape) of a given spent PWR UO_2 fuel assembly configuration is virtually solely determined by the top end region of the active zone of the fuel assemblies. To verify this expectation the axial fission density distribution along the fuel zone, as defined by eq. (6), was also calculated in the Phase II-C benchmark program,

$$\rho_i = \frac{f_i}{\sum_{j=1}^{N} f_j} \text{ with } f_i = \frac{1}{V_i}\int_{V_i} \Sigma_{fiss}(\vec{r},E)\,\Phi(\vec{r},E)\,d\vec{r}\,dE \qquad (6)$$

N:= Number of axial zones chosen to present the axial fission density distribution,

ρ_i := Fission density recorded in the i-th zone,

V_i := Volume of the i-th zone,

$\Phi(\vec{r},E)$:= Scalar flux at locus $\vec{r}$ and energy E,

Σ_{fiss} := Macroscopic fission cross-section.

As appears from Figure 1, the presence of a spacer grid in the top end region of the fuel zone impacts the shape of an axial burnup profile the more the higher the average burnup of the profile is. To take account of the impact of this "local asymmetry" of the profile on the neutron multiplication factor k_{eff} (shape) and hence the end effect eq. (1) the "local asymmetry parameter"

$$LA(\mu) = \frac{S13(\mu)}{S6(\mu)} \text{ with } S13(\mu) = \frac{1}{n}\sum_{\nu=1}^{3} \alpha_{\nu\mu},\ n = 32 \qquad (7)$$

has been used in the evaluation of the Phase II-C benchmark results [3].

For the Phase II-C benchmark the burnup groups 3 and 6 were used, cf. Figure 2. Two profiles named as "B32A222222" and "B50A222222" were formed as references cases by using the upper bounds 32 MWd/kg U and 50 MWd/kg U, respectively, of the two burnup groups as average burnup values and the average $\alpha_{\nu\mu}$ values of all the 850 axial burnup profiles (these values are given by the normalized profile specified as "total" in Figure 2). From each reference case a set of profiles was derived by replacing successively the $\alpha_{\nu\mu}$ values of nodes 1 through 6 of the reference case by the group-specific minimum or maximum $\alpha_{\nu\mu}$ values observed in Ref. [6] and by taking into account the normalization condition eq. (5). Figure 3 shows the reference cases and the profiles with the highest asymmetry (BbbA111111 with bb = 32 and 50, respectively) and the lowest asymmetry thus obtained (BbbA333333 with bb = 32 and 50, respectively). (The digit "n_ν" in the profile's identification name "$BbbAn_1n_2n_3n_4n_5n_6$" is taken to be 2, when the total average $\alpha_{\nu\mu}$ value is used for the ν-th node, is set to 1, when the group-specific minimum $\alpha_{\nu\mu}$ value is applied to the ν-th node, and is chosen to be 3, when the group-specific maximum $\alpha_{\nu\mu}$ value is used for the ν-th node.)

For the Phase II-C calculations a transport cask was used (cf. Figures 4 and 5), containing 21 fuel assemblies separated by borated stainless steel (shown in black color in Figures 4 and 5) and assumed to be completely flooded with pure lightwater.

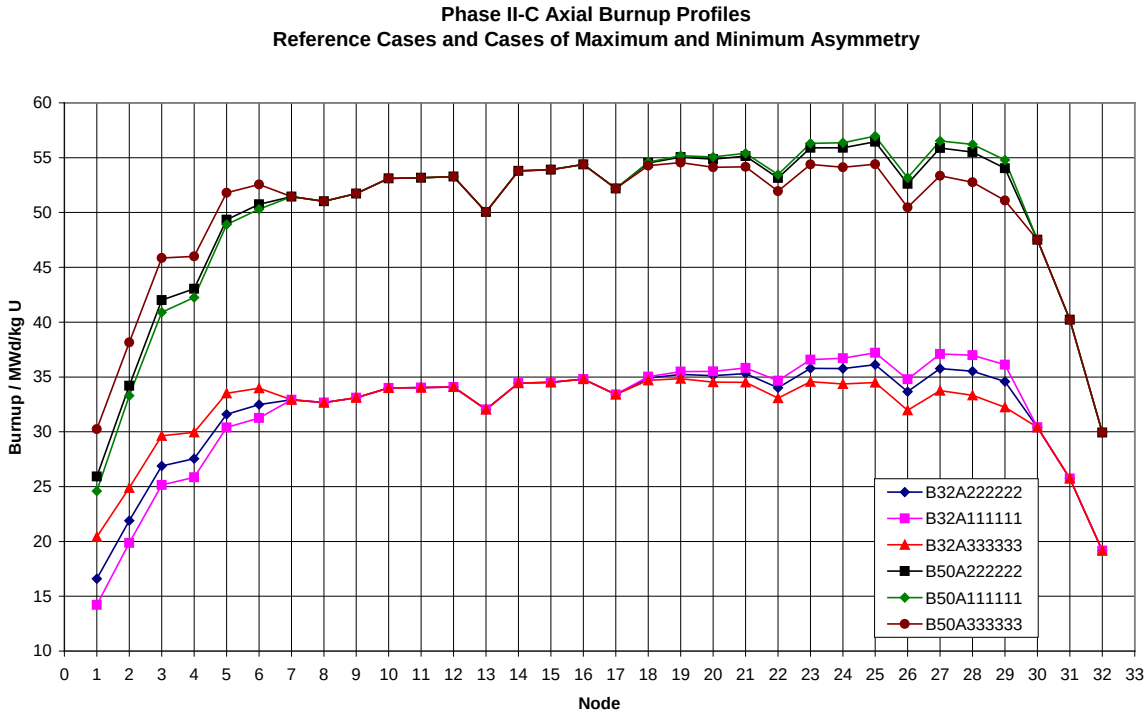

Figure 3

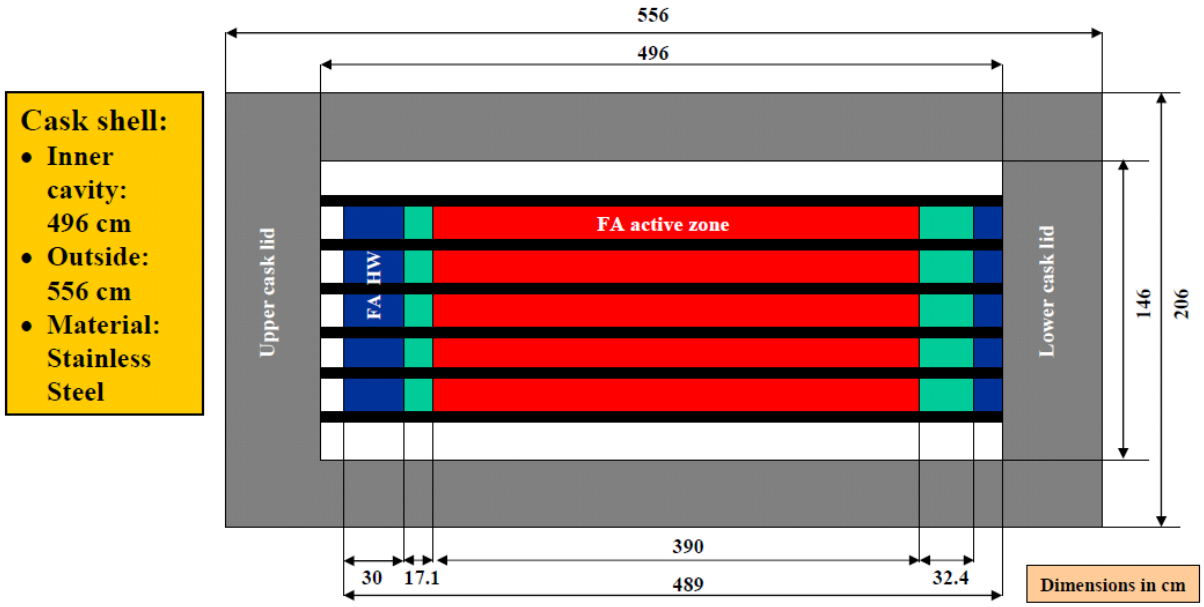

Figure 4

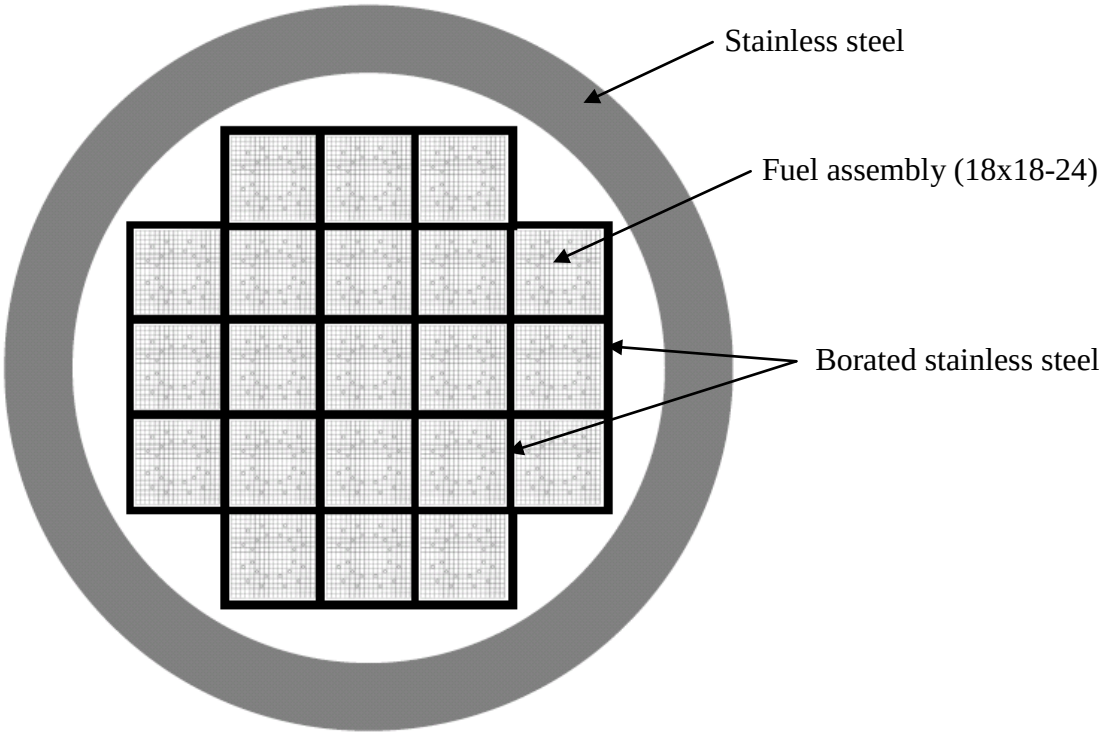

Figure 5

2.2 Summary of the results

The results obtained for the end effect are presented in Figure 6. As appears from this Figure, the dependence of the end effect on the top end parameter eq. (2) can be described by simple linear regression functions r_{B32} for the average burnup B = 32 MWd/kg U and r_{B50} for the average burnup B = 50 MWd/kg U, respectively,

$$\Delta k_{ee}(B32) = r_{B32}(S6) \quad \text{and} \quad \Delta k_{ee}(B50) = r_{B50}(S6) \ . \tag{8}$$

The following remarkable relationship between the end effects $\Delta k_{ee}(B50)$ at the average burnup B = 50 MWd/kg U and $\Delta k_{ee}(B32)$ at average burnup B = 32 MWd/kg U has been found, cf. [3]:

$$\left.\begin{aligned} \Delta k_{ee}(B50) &\approx r_{B32} \cdot \beta + \delta k \\ \Delta k_{ee}(B32) &\approx \beta^{-1} \cdot (r_{B50} - \delta k) \end{aligned}\right\} \text{ with } \beta = \frac{50}{32} \text{ and } \delta k = 0.02 \ . \tag{9}$$

As appears from Figure 6, the end effect increases,

- at given burnup, with increasing asymmetry and,
- at given asymmetry, with increasing average burnup.

The values of the sample correlation coefficient R^2 of the regression functions r_{B32} and r_{B50}, respectively, are indicated in Figure 6. As can be seen, the R^2 value achieved for r_{B50} is signifi-

cantly lower than the R^2 value obtained for r_{B32}. This is due to the fact, that the impact of the "local asymmetry" of the profile's shape at the top end of the profile increases with increasing average burnup of the profile, as it is to be expected from Figure 1. This can be verified by plotting the observed $\Delta k_{ee}(B32)$ and $\Delta k_{ee}(B50)$ values against the parameter

$$A = S6 + g \cdot LA = S6 + g \cdot \frac{S13}{S6}, \tag{10}$$

cf. Figure 7. The factor g in eq. (10) couples the profile's asymmetry with the "local asymmetry" of the profile's top end shape. In the "uncoupled" case, i.e. with $g = 0$ one gets the regression curves presented in Figure 6. In Figure 7 these curves serve as starting curves, and the coupling factor g is then increased such that the sample correlation coefficient R^2 of the resultant regression functions is maximized. As appears from Figure 7, the increase in R^2 obtained for the 32 MWd/kg U axial profiles is negligible, whereas the increase in R^2 found for the 50 MWd/kg U axial profiles is significant. This confirms that

- the impact of the "local asymmetry" on the end effect increases with increasing average burnup.

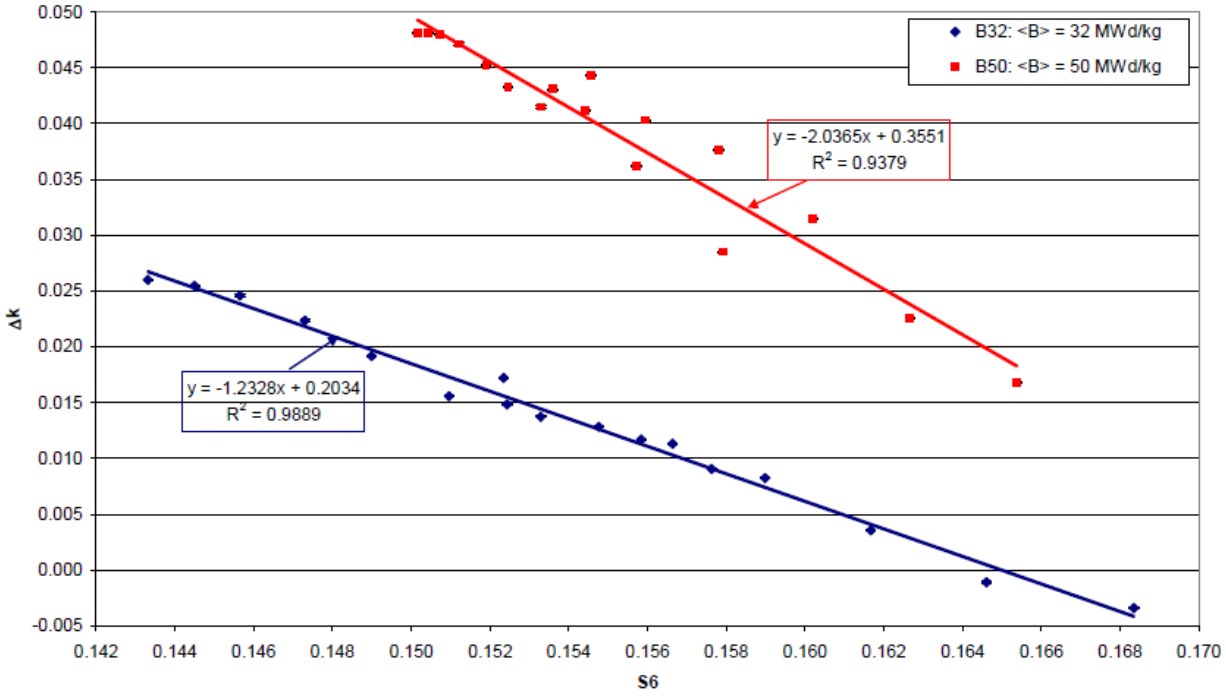

***Figure 6**: Regression analysis of the observed end effect values $\Delta k_{ee}(B32)$ and $\Delta k_{ee}(B50)$ as a function of the top end parameter S6*

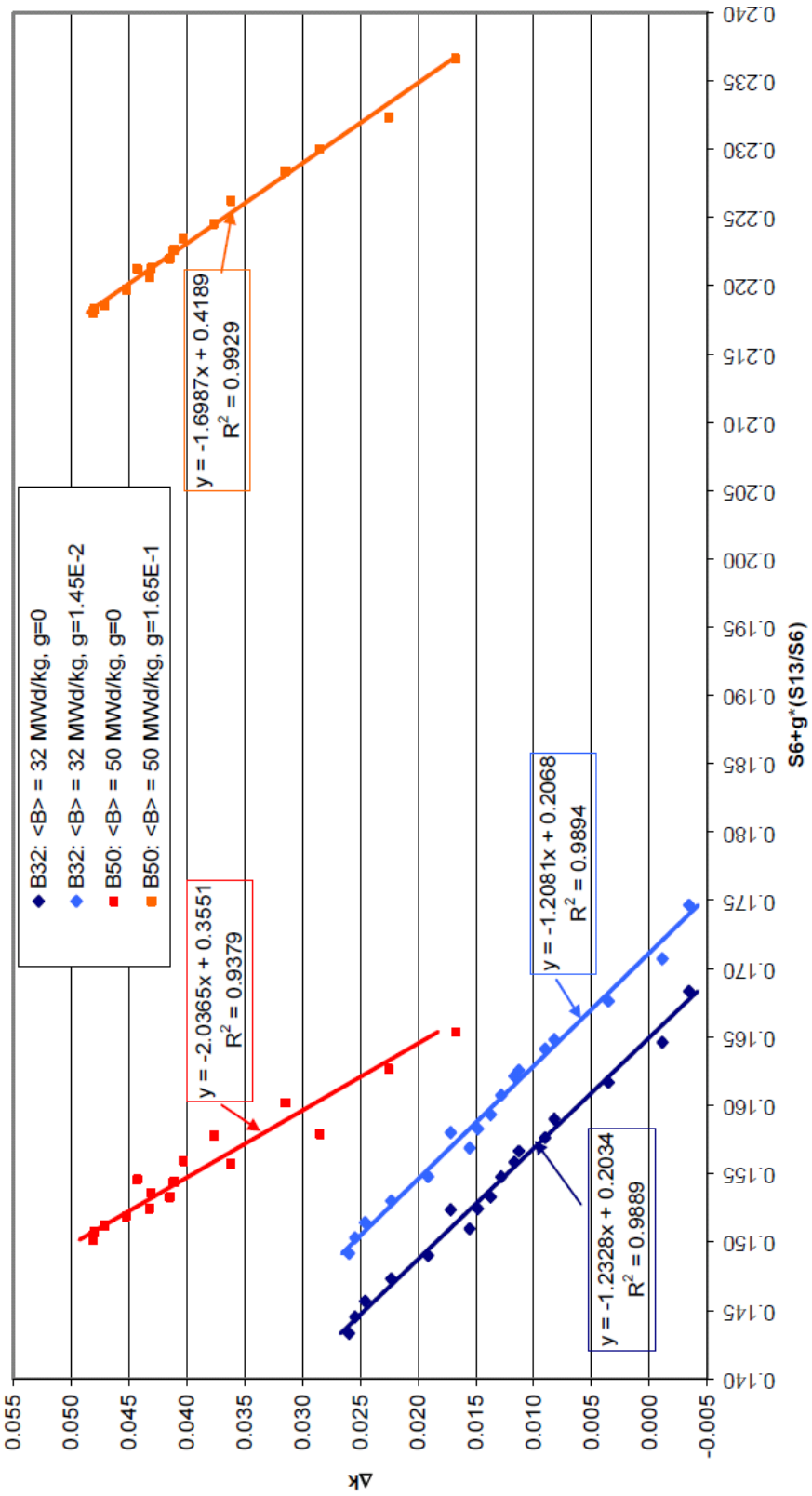

***Figure 7**: Regression analysis of the observed end effect values Δk_{ee}(B32) and Δk_{ee}(B50) as a function of the parameter S6+g·LA, cf. eq. (10)*

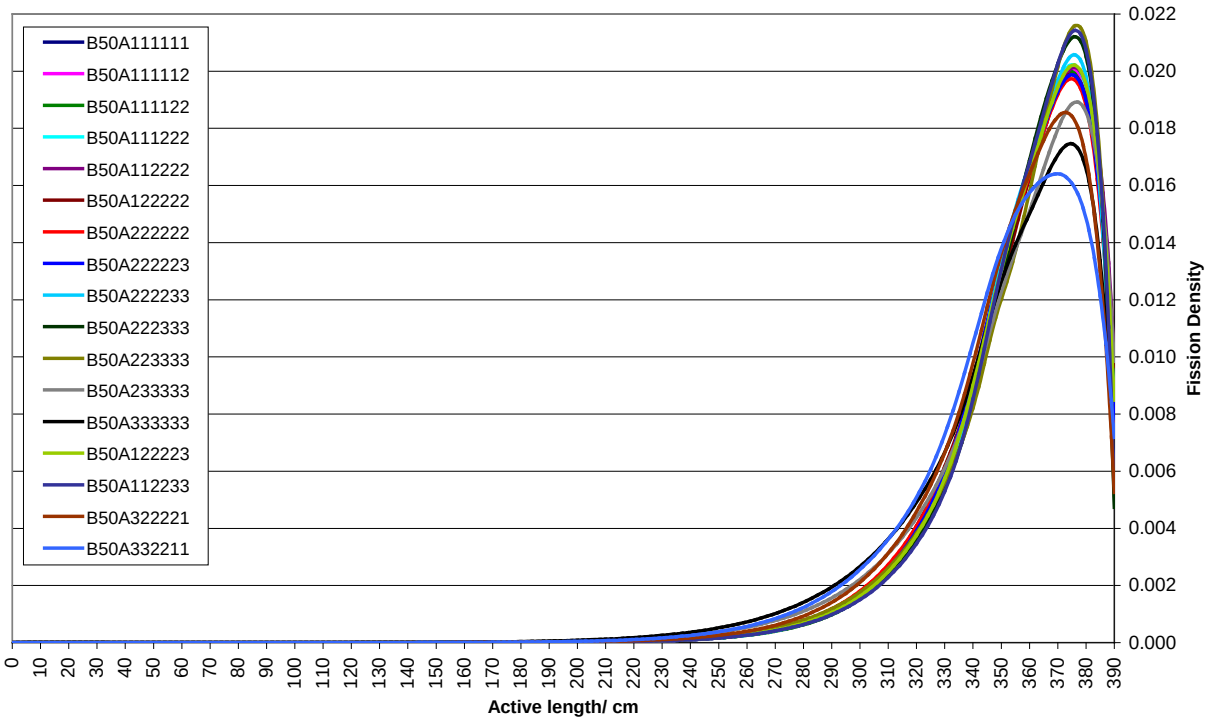

***Figure 8**: Normalized fission density distributions obtained for the profiles with 50 MWd/kg U average burnup*

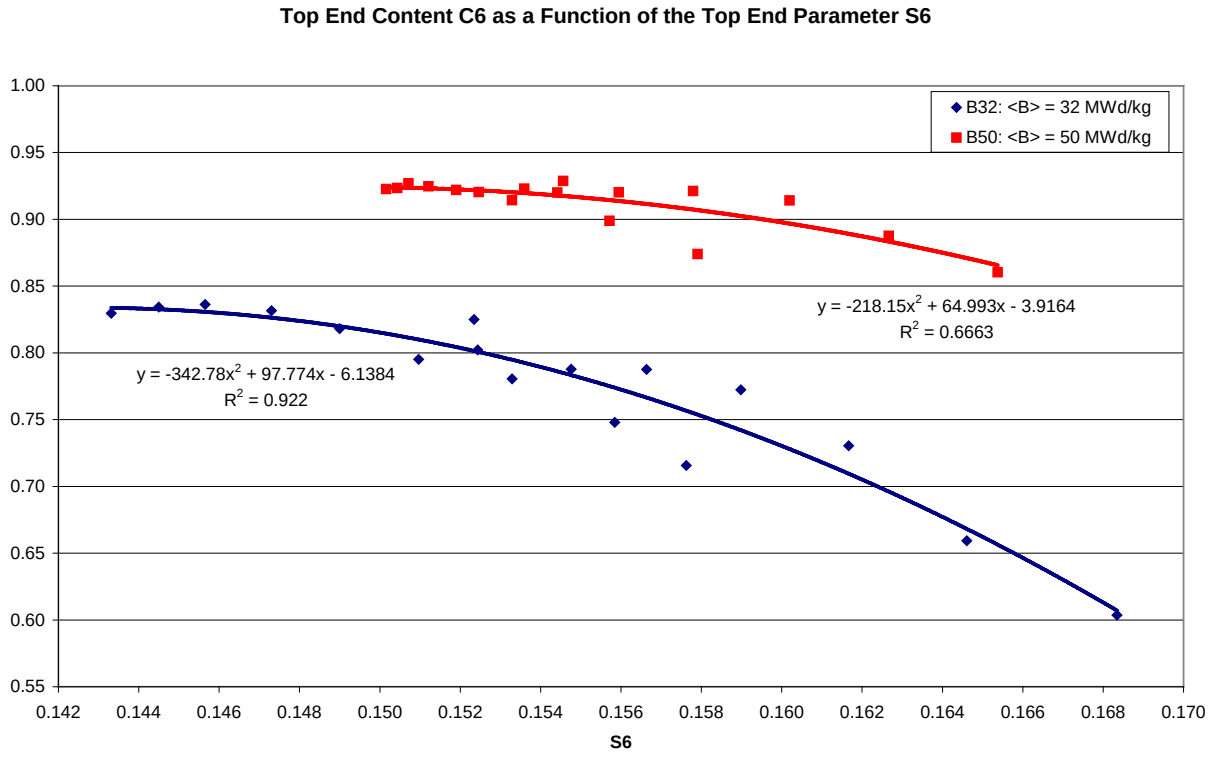

***Figure 9**: Regression analysis of the C6 values obtained for the Phase II-C axial burnup profiles*

Figure 8 shows the normalized least-squares fit curves $f(z)$ obtained from the observed fission densities eq. (6). As expected, the fission density distributions are strongly peaked in the top end region of the fuel zone, and they are shifted the more towards the top end of the active length the higher, at given burnup, the asymmetry of the profiles is and the higher, at given asymmetry the average burnup is. This can be demonstrated by plotting the "top end content"

$$C6 = \int_{\zeta_6}^{L} dz\, f(z) \text{ with } \zeta_6 = \frac{z_6 + z_7}{2} \tag{11}$$

of the fission density distributions $f(z)$ against the top end parameter S6, cf. Figure 9. L in eq. (11) denotes the active length of the fuel assemblies, and z_j is the distance of the locus of the j-th node from the bottom end of the active zone.

As discussed in detail in Ref. [3], the "scattering" of the C6 values obtained for the analyzed axial burnup profiles around the regression curves presented in Figure 9 is due to the "local asymmetry" of the profiles' shape.

Figure 10 shows the fission density distribution of the uniform burnup distribution of the average burnup which is typically cosine-shaped, irrespective of what the amount of the average burnup is. In fact, also the axial flux distribution and hence the axial fission density distribution of an unirradiated fuel assembly having a homogeneous initial enrichment distribution is cosine-shaped. Therefore, in an operating PWR core, the fuel near the axial center of the assembly is

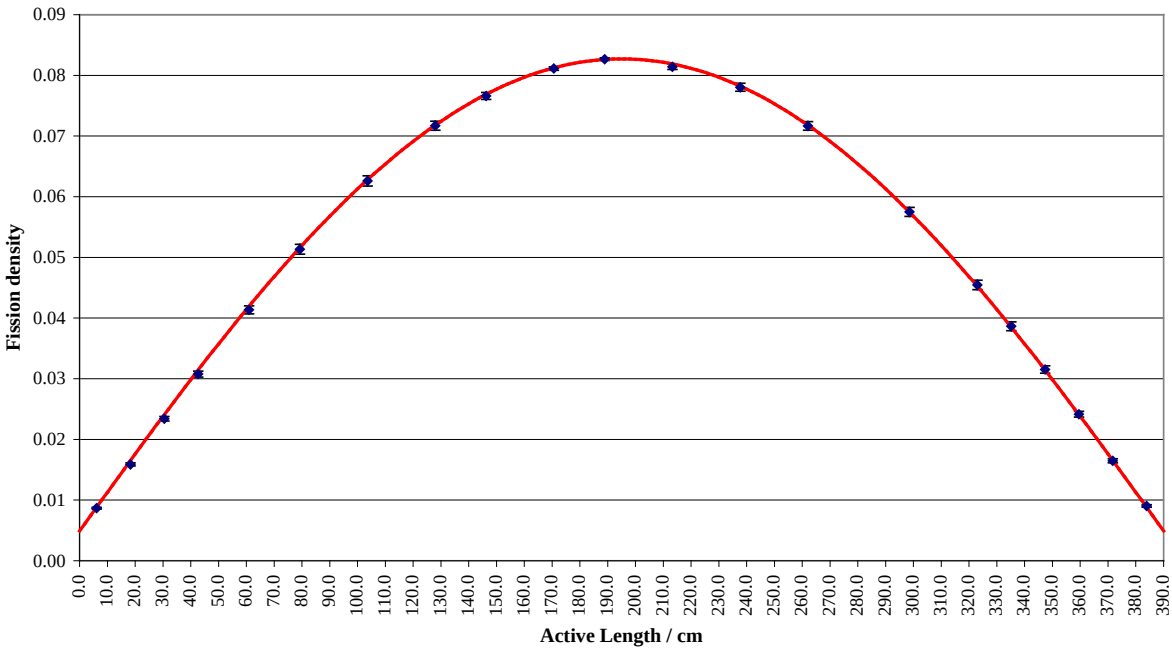

***Figure 10**: Non-normalized axial fission density distribution typical of uniform burnup distributions*

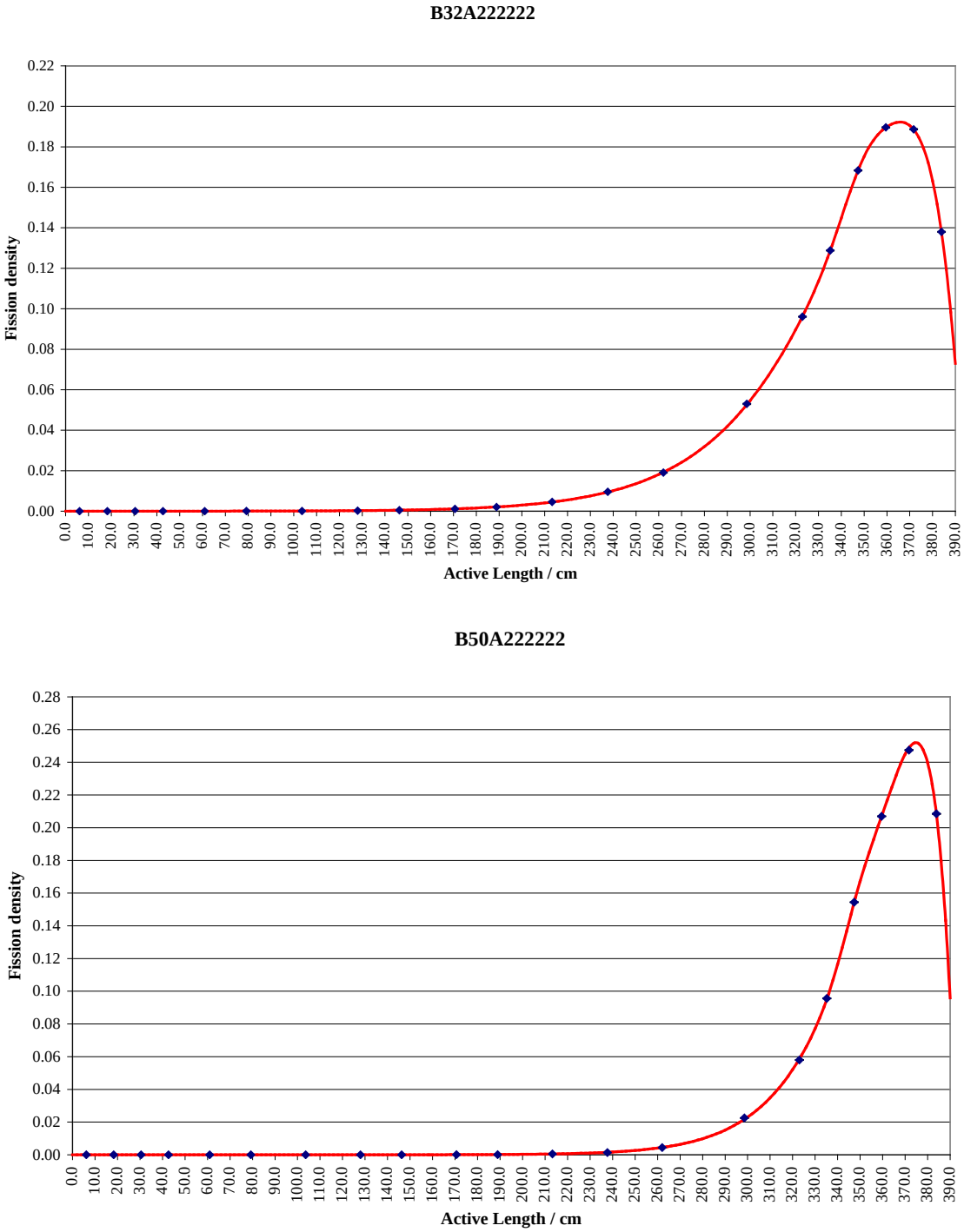

***Figure 11**: Comparison of the non-normalized fission density distributions obtained for the reference profiles B32A222222 and B50A222222*

depleted at a faster rate than at the ends of the fuel zone. With increasing burnup the flux shape flattens out due to the higher fuel depletion and fission product poisoning near the center. Accordingly, due to increase of spectrum hardening from the bottom end to the top end of the fuel zone (cf. section 2.1) the axial fission density distribution of the fuel assembly outside of the core becomes more and more peaked in the top end region of the fuel zone. Figure 11 demonstrates, in addition to Figure 9, that the fission density distribution is shifted the more towards the top end of the fuel zone the higher, at given asymmetry the average burnup is. This observation is in agreement with the result that, at given asymmetry, the end effect increases with increasing average burnup.

3 The Phase II-E benchmark

3.1 Brief description of the benchmark

The two bounding axial burnup profiles generated from a non-public database of axial burnup profiles of 17x17-25 UO_2 fuel assemblies by means of the methods described in [5] are presented in Figure 12. One profile is related to an average burnup of 30 MWd/kg U, the other is related to an average burnup of 50 MWd/kg U. Both profiles are given on 35 nodes. Since the active length of the 17x17-25 fuel assemblies amounts to L = 365.76 cm κ = 7, together with n = 35, is now

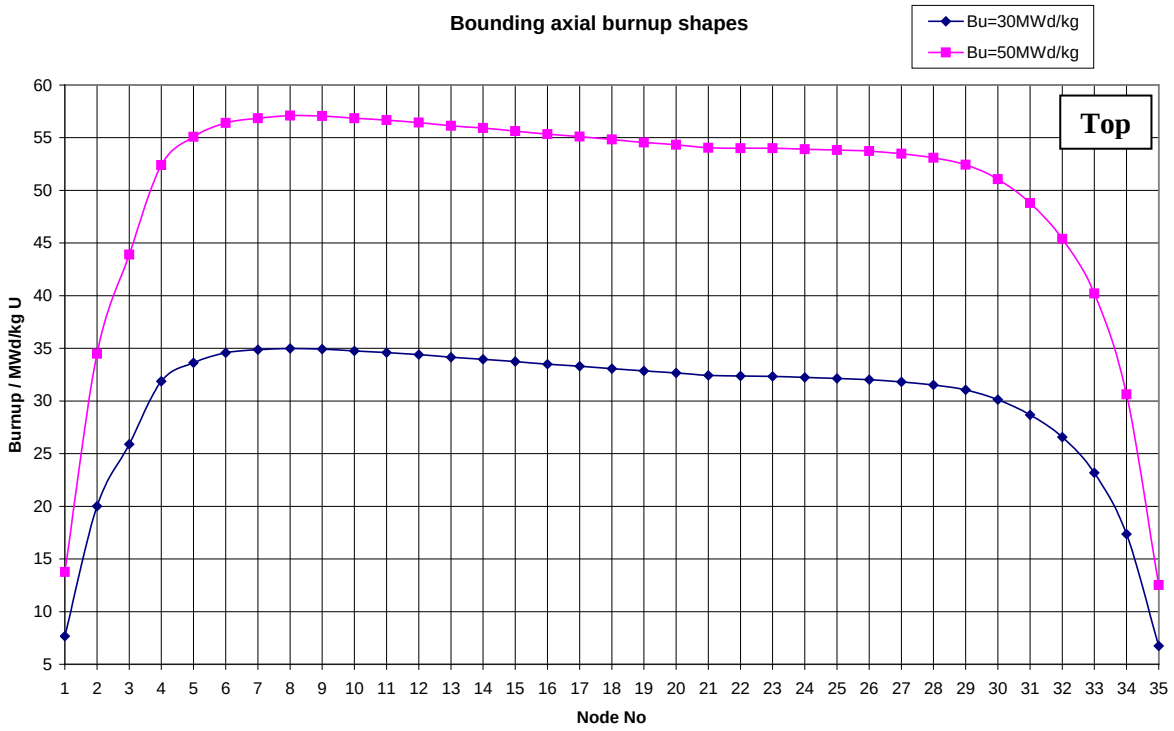

***Figure 12**: Axial burnup profiles chosen for the Phase II-E benchmark program*

chosen in eq. (2) since the S7-length of (7/35)·365.76 cm = 73.152 cm is nearly the same as the S6-length of (6/32)·390 cm = 73.125 cm used in the Phase II-C analysis. As appears from Figure 12, the impact of spacer grids on the shape of the profiles has been neglected in the Phase II-E benchmark exercise.

For Phase II-E virtually the same transport cask configuration have been assumed as were used in Phase II-C, cf. [8]. The cask contains 21 fuel assemblies separated by borated stainless steel (cf. Figure 5) and is assumed to be completely flooded with pure lightwater. The neutron multiplication factor of this cask configuration and the related end effect were analyzed as a function of the control rod (CR) insertion depth d_{CR} in the assemblies' fuel zone during depletion. So, for CR insertion depths $0 < d_{CR} < L$ the fuel zone of the fuel assemblies was divided into two zones, the zone at the top end of the fuel zone which was exposed to CR insertion during depletion, and the remainder of the fuel zone which was not exposed to CR insertion. Accordingly, the axial burnup profiles shown in Figure 12 as well as the uniform burnup distribution of the average burnup values of the profiles were divided into these two zones.

3.2 Results

3.2.1 Conclusions from the Phase II-D and Phase II-C benchmark results

As known from the Phase II-D benchmark exercise [4], CR insertion leads, due to spectrum hardening, to a significant increase in the number densities of ^{235}U and ^{239}Pu and hence to a significant increase in the fuel's reactivity compared to the case of no CR insertion. The increase in the number densities of ^{235}U and ^{239}Pu and hence the increase in reactivity increases with increasing burnup since increasing burnup results in increasing spectrum hardening [9]. So, the increase in the reactivity importance due to CR insertion increases faster in axial fuel zones with higher depletion rates and hence higher burnups. From that it follows that the impact of CR insertion on the neutron multiplication factor of a PWR UO_2 configuration of interest and hence on the end effect related to a given axial burnup profile is strongly dependent on the CR insertion depth during depletion. In particular it can be expected that full CR insertion into the entire fuel zone of a fuel assembly during depletion results, compared to the case of no CR insertion, in a significant increase of the configuration's neutron multiplication factor but, at the same time, in a significant decrease of the end effect since the reactivity importance of the center zone of the fuel zone increases faster with increasing spectrum hardening than the reactivity importance of the end zones of the fuel zone.

Conclusions on the changes of the configuration's neutron multiplication factors k_{eff} (shape) and k_{eff} (unif. dist.) and hence, according to eq. (1), on the change of the end effect with changing CR insertion depth can be drawn from the outcomes of the Phase II-C benchmark by following simply, from the top end to the bottom end of the fuel zone, the fission density distribution f(z) associated with the given axial burnup profile at zero CR insertion depth (cf. Figure 11, for instance) and by starting, at zero CR insertion depth, with the fission density distribution of the uniform distribution of the profile's average burnup (cf. Figure 10, for instance).

In fact, to predict the behavior of k_{eff} (shape) qualitatively, one needs only to follow the increase of the probability content

$$C(\varsigma) = \int_{L-\varsigma}^{L} dz\, f(z) \tag{12}$$

as given by the fission density distribution f(z) with increasing distance ς from the top end of the fuel zone:

- As appears from Figure 11 for example, at the beginning, i.e. at small CR insertion depths $\varsigma = d_{CR}$, the fission probability $C(\varsigma)$ increases very rapidly with increasing ς, and it is therefore to be expected that the neutron multiplication factor k_{eff} (shape) rapidly increases since the number densities of ^{235}U and ^{239}Pu in the region $[L-\varsigma, L]$ are increased due to CR insertion, actually the more the higher the burnup becomes with increasing $\varsigma = d_{CR}$.
- Then, with further increasing CR insertion depth $\varsigma = d_{CR}$ the increase of the fission probability $C(\varsigma)$ slows down due to the shape of the fission density distribution; and when ς exceeds the value ς_M where the maximum of the fission density distribution is located, then the increase in $C(\varsigma)$ goes down more and more. It is therefore to be expected that the neutron multiplication factor k_{eff} (shape) still increases, but that the amount of its increase slows down more and more with increasing insertion depth $\varsigma = d_{CR}$.
- Finally, when $\varsigma = d_{CR}$ reaches a certain value ς_P such that the region $[L-\varsigma_P, L]$ virtually contains the entire fission density peak then any increase in ς results in a negligible increase of $C(\varsigma)$ only, and it is then to be expected that k_{eff} (shape) virtually remains constant for any value $\varsigma > \varsigma_P$.

The values ς_M and ς_P tend to decrease with increasing average burnup (cf. Figure 11). It is therefore to be expected that both, the rapidity with which the neutron multiplication factor k_{eff} (shape) increases with increasing insertion depth $\varsigma = d_{CR}$ at the beginning of the CR insertion, and the rapidity with which k_{eff} (shape) converges towards a certain case-specific limit, increase with increasing average burnup.

Of course, CR insertion affects the shape of a fission density distribution for a given axial burnup profile. In addition, CR insertion may impact the shape of the axial burnup profile and increase the asymmetry of the profile in particular. Nevertheless, for a given axial burnup profile (given, for instance, by a bounding profile as needed for the determination of a burnup credit loading curve [9]) the associated fission density distribution at zero CR insertion is, so to speak, the "starting condition" which significantly affects the rapidity with which k_{eff} (shape) can change due to the changes in the axial isotopic composition distribution caused by CR insertion.

In fact, the cosine-shaped fission density distribution associated with the uniform distribution of the average burnup (cf. Figure 10) provides a completely different "starting condition". Before a significant response of the neutron multiplication factor k_{eff} (unif. dist.) to a change in the isotopic

composition due to CR insertion can be expected a significant increase in the fission density must occur at the top end of the fuel zone. This requires a sizeable insertion depth $\varsigma = d_{CR}$ since a potential increase in the reactivity due to the change in the isotopic composition at the top end region of the fuel zone competes with increased leakage due to the close proximity to the end of the fuel zone. In other words, a significant "reorientation" of the fission density distribution such that a proper peak of the fission density in the top end region of the fuel zone can be obtained requires a proper CR insertion depth $\varsigma = d_{CR}$. Therefore, it is to be expected that the neutron multiplication factor k_{eff} (unif. dist.) starts to increase at a significantly higher $\varsigma = d_{CR}$ value than the neutron multiplication factor k_{eff} (shape).

After the neutron multiplication factor k_{eff} (unif. dist.) has started to increase k_{eff} (unif. dist.) will continue to increase with any further increase of the CR insertion depth ς till $\varsigma = L$ is reached. This is due to the fact that any increment $\Delta\varsigma$ in the insertion depth ς means that in the range $[\varsigma, \varsigma + \Delta\varsigma]$ one uniform isotopic composition is exchanged for another isotopic composition which has a higher reactivity due to spectrum hardening. This exchange is always the same for any interval $[\varsigma, \varsigma + \Delta\varsigma]$ since a uniform burnup distribution is examined. After a certain insertion depth is reached the increase in the neutron multiplication factor will slow down more and more since the relative increase of the axial length of the fuel zone containing already the more reactive isotopic composition is decreasing with increasing ς according to $1/(1+\varsigma/\Delta\varsigma)$. And finally, the maximum of the fission density distribution will return, step by step, with increasing ς to the center of the fuel zone, till at $\varsigma = L$ the fission density distribution is again cosine-shaped.

So therefore, because the neutron multiplication factor k_{eff} (unif. dist.) starts to increase at a higher insertion depth ς than the neutron multiplication factor k_{eff} (shape) and because k_{eff} (unif. dist.) does not stop to increase – even if the amount of the increase is slowing down more and more for higher ς values – till $\varsigma = L$ is reached, whereas k_{eff} (shape) reaches its case-specific limit at a ς value which is significantly lower than L, it can be inferred that the end effect, given according to eq.(1), has a maximum at a relatively low ς value, which decreases with increasing average burnup. In addition, since the increase in the fuel's reactivity due to the spectrum hardening caused by CR insertion increases with increasing burnup it is to be expected, as already stated, that the end effect is lower for the case $\varsigma = L$ than for the case $\varsigma = 0$.

3.2.2 Summary of results

As appears from Figures 13 through 20, all the predictions made in the preceding section are confirmed by the outcomes obtained in the Phase II-E benchmark calculations:

- Starting with the CR insertion the neutron multiplication factor k_{eff} (shape) responds nearly promptly and increases very rapidly; and the response of k_{eff} (shape) is the prompter the higher the average burnup is (cf. Figures 13 and 15). Then, around a CR insertion depth d_{CR} where the maximum of the axial fission density distribution is located (cf. Figure 14, for example) the increase of k_{eff} (shape) begins to slow down; and for insertion depths d_{CR} greater than

approx. 100 cm, where most of the fission density distribution is already covered by the integral eq. (12), no further increase of k_{eff} (shape) is observed (cf. Figures 13 and 15).

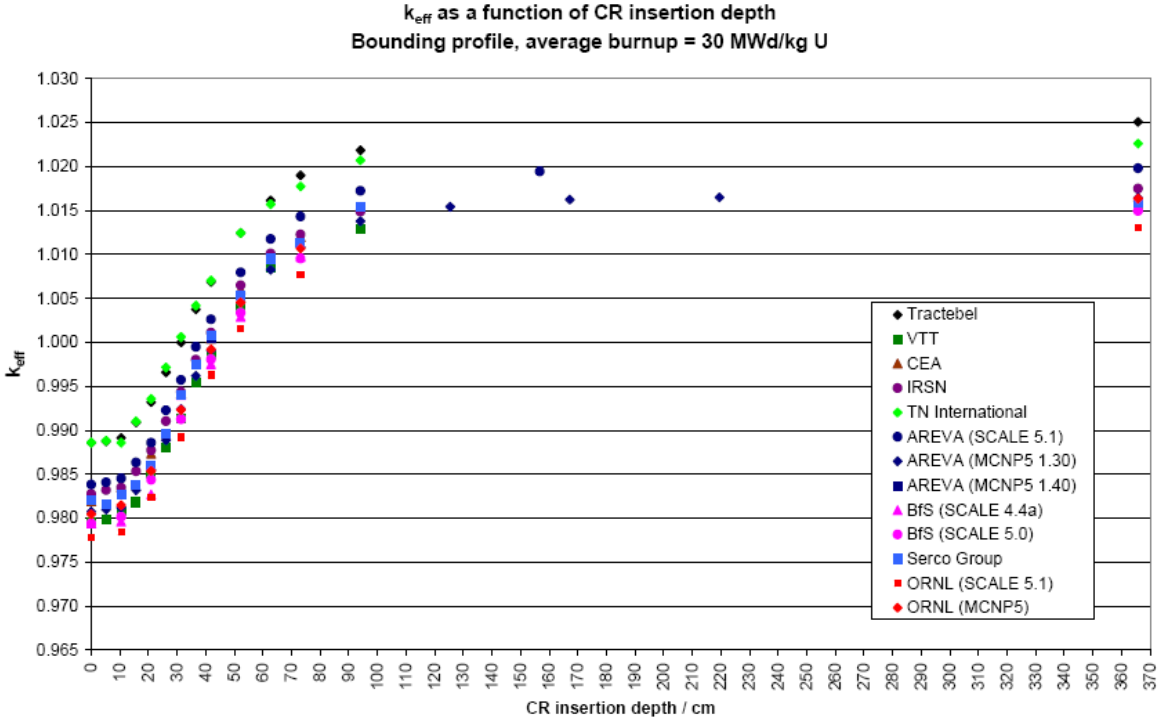

Figure 13

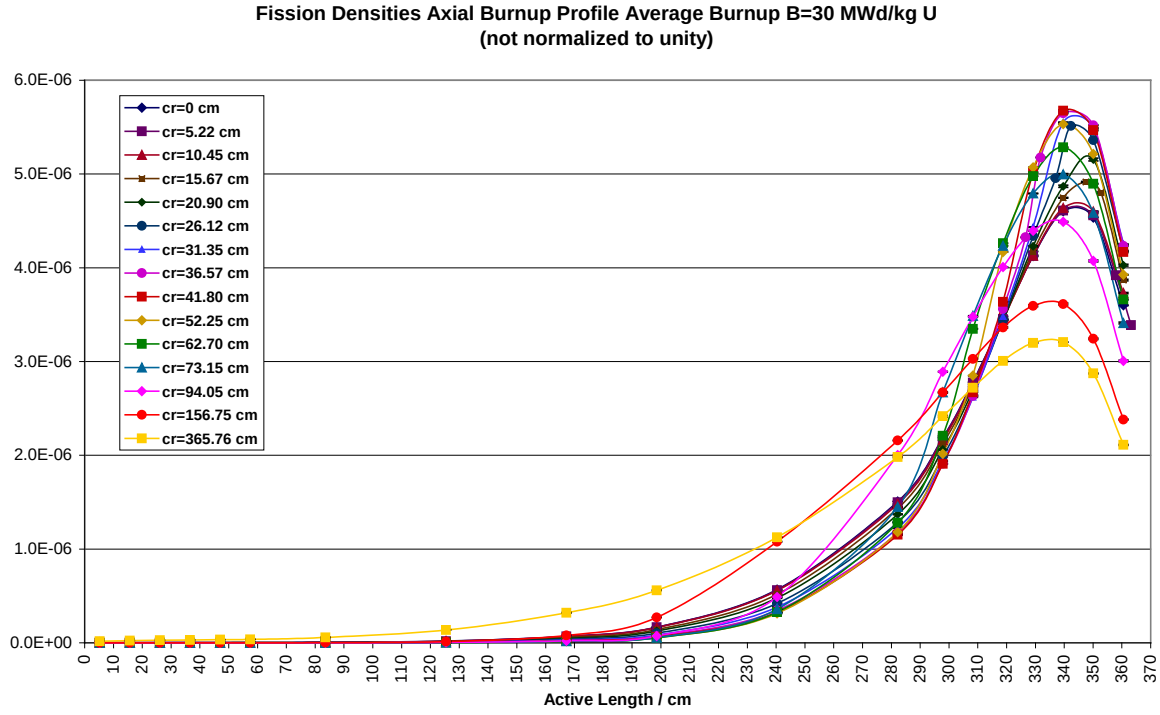

Figure 14

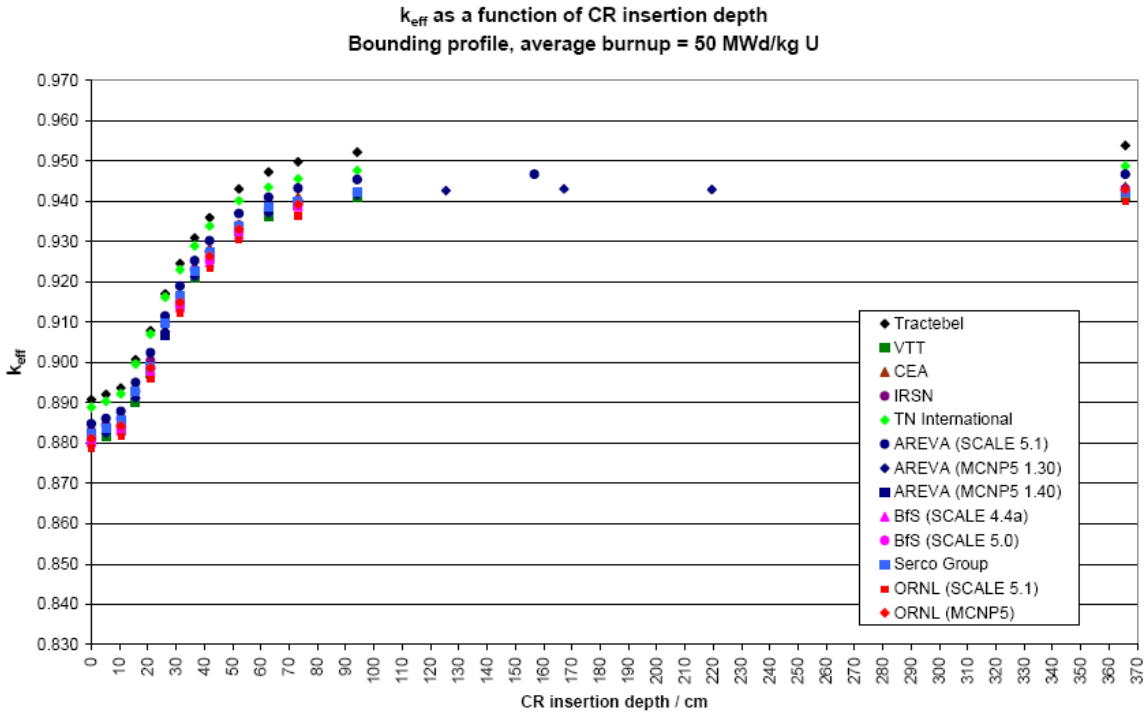

Figure 15

- In contrast to the behavior of k_{eff} (shape) the response of the neutron multiplication factor k_{eff} (unif. dist.) of the uniform burnup distribution is "delayed", i.e. a sizeable insertion depth d_{CR} has to be reached before a significant increase in k_{eff} (unif. dist.) can be observed (cf. Figures 16 and 18). Then, after a sufficient "reorientation" of the fission density distribution is reached (cf. Figure 17, for example), k_{eff} (unif. dist.) starts to increase rapidly due to a more and more pronounced peaking of the fission density distribution in the top end region of the fuel. With increasing CR insertion depth more and more of the content below the fission density distribution is covered by the integral eq. (12) even though the peaking of the fission density distribution becomes less and less pronounced. The increase in k_{eff} (unif. dist.) slows down, therefore, expressing the fact that the relative increase of the axial length of the fuel zone containing already the more reactive isotopic composition is decreasing with increasing CR insertion depth. However, as expected, the increase in k_{eff} (unif. dist.) is continued till $d_{CR} = L$ is reached (cf. Figures 16 and 18).

- Consequently, as expected, starting the CR insertion the end effect first increases significantly, reaches then a maximum and slows down till it reaches at full CR insertion a value which is lower than the value of the end effect at zero CR insertion (cf. Figures 19 and 20).

As appears from Figure 19, in case of the average burnup of 30 MWd/kg U the end effect becomes negative for full CR insertion. A negative end effect means that the so-called "bounding profile" is not longer bounding. The use of a so-called "bounding profile" at a negative end effect results in an underestimation of the neutron multiplication factor of a fuel system of interest. So,

one should be cautious with the use of so-called bounding profiles when CR insertion has to be considered. *The bounding profile at negative end effect is the uniform burnup distribution*. This goes irrespective of whether CR insertion has to be taken into account or not.

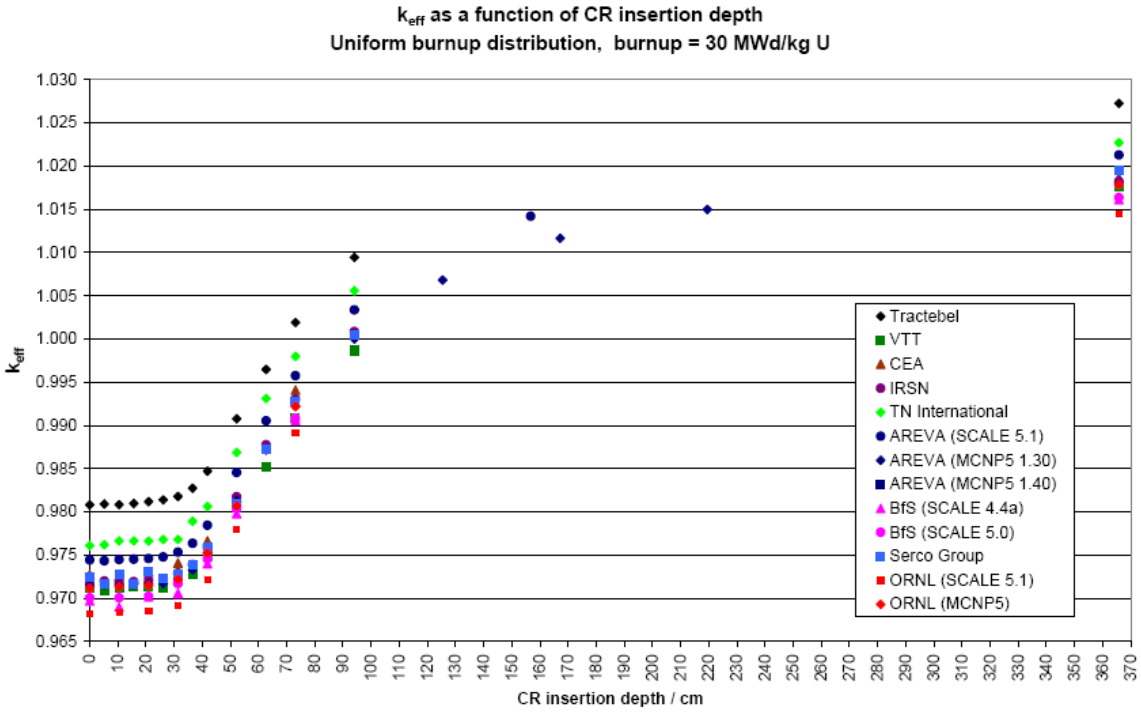

Figure 16

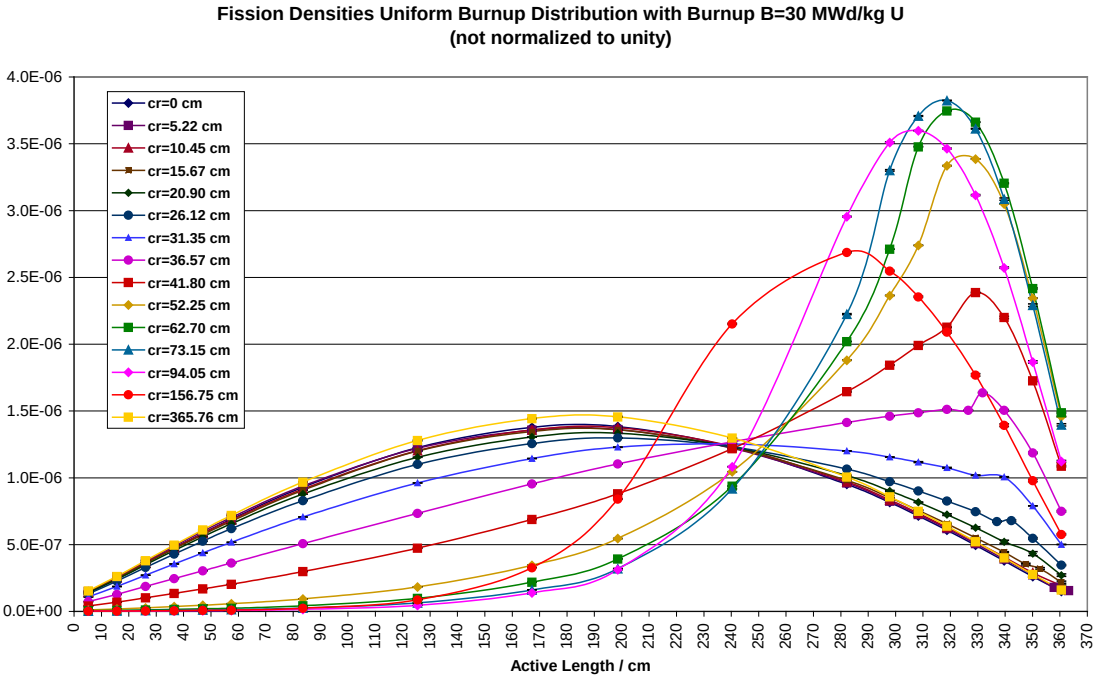

Figure 17

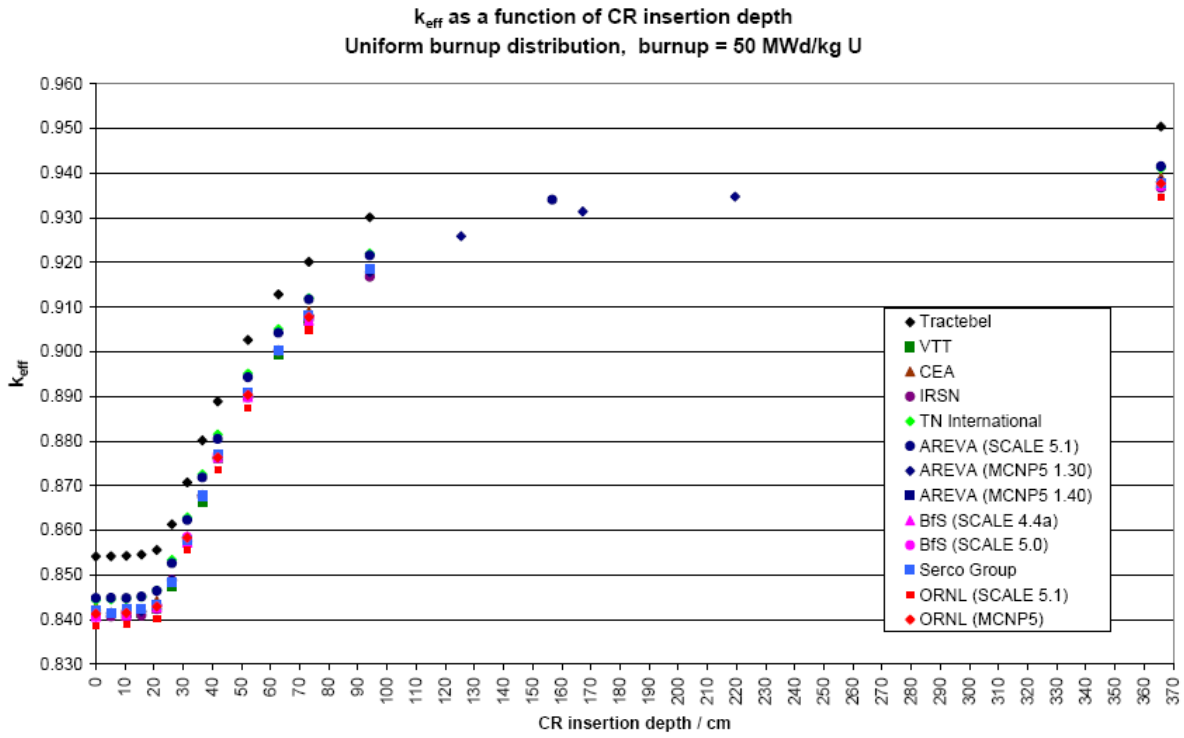

Figure 18

So, one of the lessons that can be learnt from the results of the Phase II-C through Phase II-E benchmarks is

- that it is of course necessary in burnup credit applications to look for bounding axial burnup profiles (cf. [5] and [9]),
- but that it is also necessary to control whether the end effect obtained with a so-called "bounding profile", is negative or not.

If the end effect is negative the uniform burnup of the average burnup of the profile is the bounding profile. *A non-uniform burnup distribution can only be bounding, if the end-effect obtained with this distribution, is not negative*.

Another lesson that can be learnt from Phase II-E in particular is that relatively small CR insertion depths have to be considered in burnup credit applications. It is in fact common practice in core operation that at least one CR bank is in a "target bite position", i.e., at begin of cycle the control rods of this CR bank are inserted into the fuel zone of the involved fuel assemblies with an insertion depth of usually not more than about 30 cm, and the insertion depth is then gradually reduced during the cycle and tends towards zero at the end of cycle (cf. [7] for example).

It is also quite common practice in core operation to use extended low power operation at the end of cycles. Then the control rods of at least one CR bank are inserted with a significant insertion depth [7]. As learnt from Phase II-D, the increase in reactivity of spent fuel due to spectrum

hardening due to CR insertion during irradiation is increasing with increasing burnup of the fuel because increasing burnup results in increasing spectrum hardening.

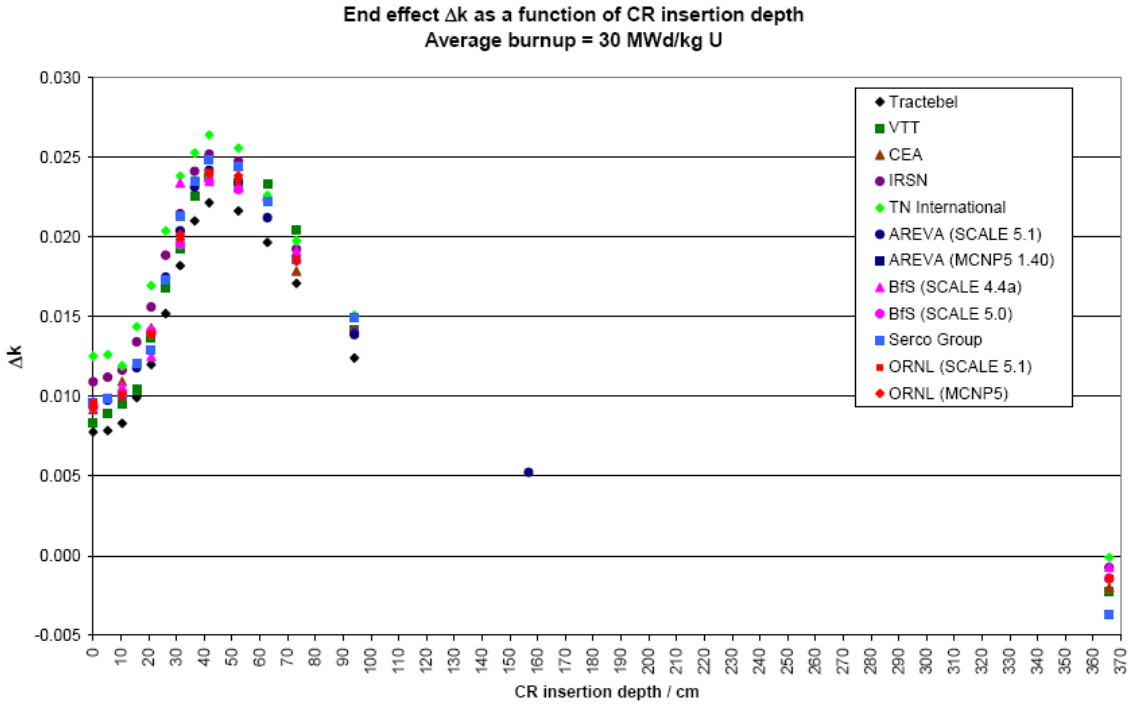

Figure 19

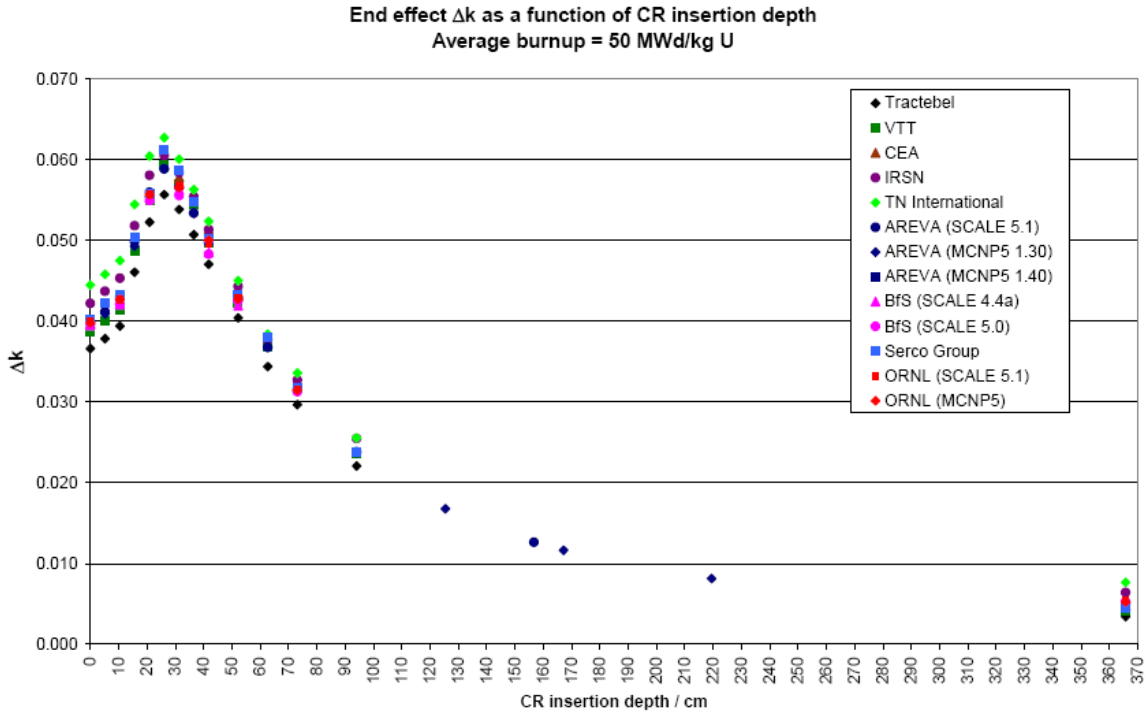

Figure 20

A further lesson that can be learnt from Phase II-C through Phase II-E benchmark results is given in the next section.

4 Observations on the case that a section of the top end of the fuel zone of the fuel assemblies juts out of the neutron absorber channels of a spent fuel storage or transport system

It has been observed that in some spent fuel storage racks of wet storage pools as well as in some spent fuel storage and transport casks the nominal length of the absorber material of the channels forming the fuel assembly storage positions is chosen equal to the nominal active length specified for the *unirradiated* fuel assemblies of the type of interest. Therefore, it can't be excluded already for the case of unirradiated fuel assemblies that, due to the manufacturing tolerances in the unirradiated fuel assemblies' active length and in the absorber length, some section of the fuel zone of the fuel assemblies juts out of the neutron absorber channels. This is however not the whole story. It has to be taken additionally into account that the active length of fuel under irradiation is increasing with increasing irradiation time, so that the active length of spent fuel can be enlarged by a factor up to about 1.008. So, assuming an active length of 365.76 cm (cf. section 3.1) plus the usual tolerance of 0.7 cm (half a pellet length) for the unirradiated fuel assembly the active length can be increased up to 369.39 cm due to irradiation. Assuming the quite common tolerance of 0.5 cm for the absorber length, it follows that a section of up to 4.13 cm of the fuel zone of the fuel assemblies may jut out of the neutron absorber channels. The question is whether such an amount of jutting-out of the absorber channels affects the neutron multiplication factor k_{eff} (shape) of the spent fuel configuration of interest or not.

Due to the outcomes of the Phase II-C benchmarks the case that the top end region of the fuel zone juts out of the neutron absorbing channels is of particular interest. Accordingly, even though the amount of the impact on the end effect may be significantly different, qualitatively the same that has been told in section 3.2.1 about the impact of CR insertion during depletion on the end effect applies to the case that the fuel zone of the fuel assemblies is only partially inserted in the absorber channels. One has only to identify now the parameter ς with the axial length of the fuel region which is not inserted into the neutron absorbing material zone. In fact starting at full coverage of the entire fuel zone, i.e. starting with a "non-coverage" of $\varsigma = 0$ the fission probability $C(\varsigma)$ due to the fission density distribution $f(z)$ associated with the applied axial burnup profile increases very rapidly with increasing ς, and it is therefore to be expected that the neutron multiplication factor k_{eff} (shape) rapidly increases due to the significant change in the neutron absorption and reflection conditions caused by the "disappearance" of the neutron absorber in horizontal direction. Then, due to the shape of the fission density distribution $f(z)$ the increase in $C(\varsigma)$ and hence the increase in k_{eff} (shape) slow down more and more, in particular when ς has exceeded the value ς_M where the maximum of $f(z)$ is located. Finally, when ς has reached the value ς_P such that the whole region $[L - \varsigma_P, L]$ which virtually contains the entire fission density peak is uncovered then k_{eff} (shape) virtually remains constant for any value $\varsigma > \varsigma_P$.

In contrast to that the "reorientation" of the fission density distribution of the uniform burnup distribution requires a sizeable non-coverage ς. Therefore, the neutron multiplication factor k_{eff} (unif. dist.) starts to increase at a significantly higher ς value than the neutron multiplication factor k_{eff} (shape). The neutron multiplication factor k_{eff} (unif. dist.) continues to increase till $\varsigma = L$ is reached, but the amount of its increase will slow down at higher ς values since the relative increase in the length of the uncovered fuel region due to an increment $\Delta\varsigma$ of this length goes down according to $1/(1+\varsigma/\Delta\varsigma)$.

So, starting at $\varsigma = 0$, it is to be expected that the end effect first increases rapidly with increasing ς, then reaches a maximum and, afterwards, decreases monotonously with further increasing ς. Of course, it cannot be expected now, in contrast to the CR insertion case, that the end effect at $\varsigma = L$ is smaller than at $\varsigma = 0$ because the increases in k_{eff} (shape) and k_{eff} (unif. dist.) are not caused by changes in the isotopic composition of the fuel.

These predictions have been checked by means of the configuration shown in Figure 21 using the axial burnup profile with 30 MWd/kg U average burnup presented in Figure 12 and assuming zero CR insertion.

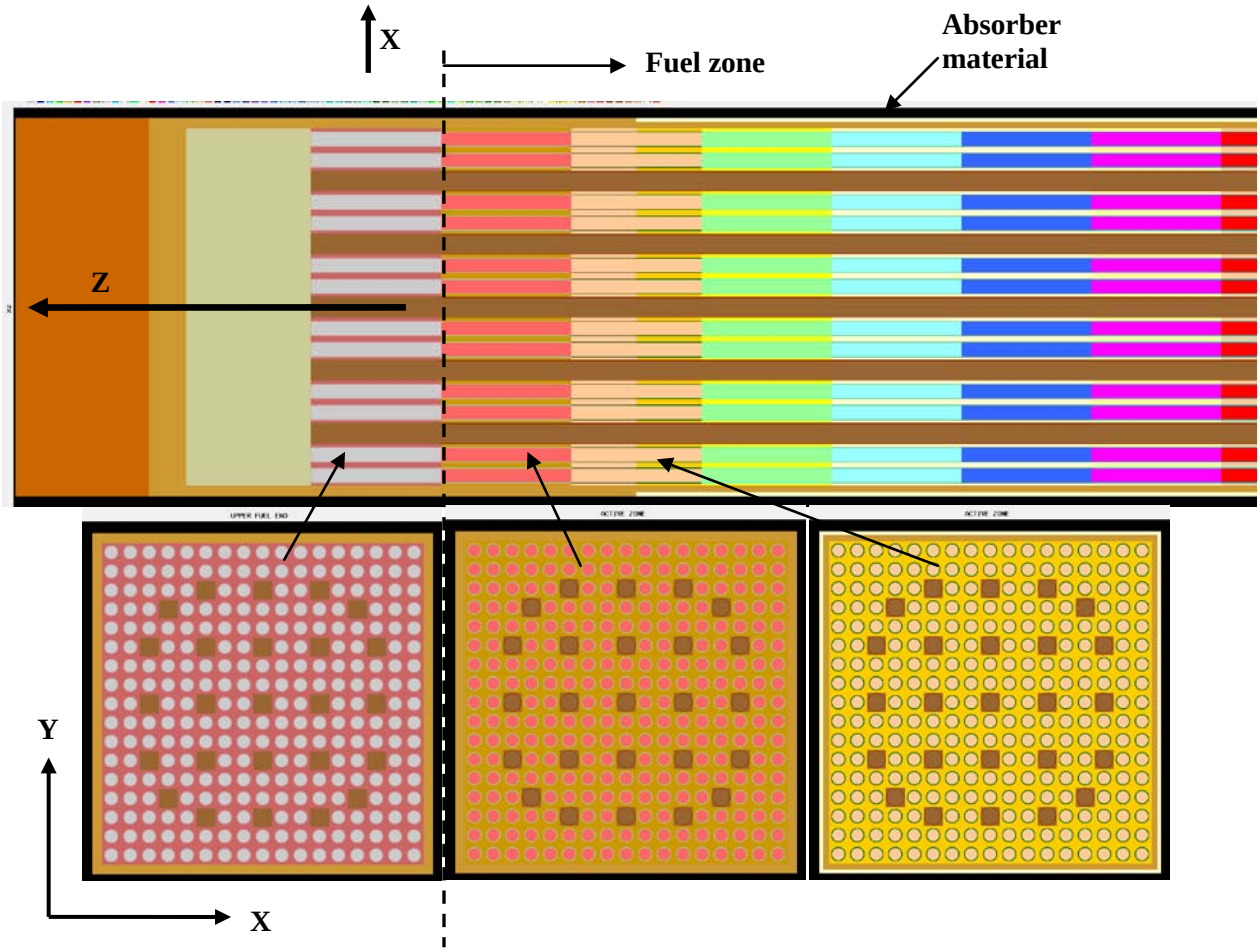

Figure 21

Figure 21 shows only the top end region of the geometry model used. This model consists of one 17x17-25 fuel assembly surrounded by the same neutron absorbing material as was used in the Phase II-E benchmark. The fuel assembly has been modeled analogously to Figure 4, but in ± Z-direction reflected by water only since no cask material was assumed. In ± X-direction and ± Y-direction the geometry model was mirror reflected so that a configuration has been simulated which is infinite in lateral extent with respect to the axial direction (± Z-direction) of the fuel assemblies. The mirror reflection boundaries were defined by the outer surfaces of the absorber channel shown in Figure 21 so that neighboring fuel assemblies in the simulated configuration were just separated by one absorber panel (as it was the case in Figure 4 or as it is usually the case in those storage racks of spent fuel ponds which are designed for burnup credit). The fuel assemblies in the simulated configuration were gradually pulled out of the absorber channels in + Z-direction; and the neutron multiplication factors k_{eff} (shape) and k_{eff} (unif. dist.) were analyzed as a function of the "non-coverage"-parameter ς.

As appears from Figure 21, first the fuel assemblies have been assumed to be completely inserted in the absorber channels so that the non-coverage parameter ς is taken to be negative at the beginning, i.e., before the pulling-out of the assemblies has been started. ς is taken to be zero when the top end of the fuel zone reaches the Z-height of the top end of the absorber channels.

The results obtained for k_{eff} (shape), k_{eff} (unif. dist.) and the end effect as a function of the non-coverage parameter ς are presented in Figure 22. As appears from this figure, the predictions made above about k_{eff} (shape), k_{eff} (unif. dist.) and the end effect as a function of ς are fully confirmed.

It is worthwhile to note that k_{eff} (shape) already responds slightly at negative ς values to the increase of ς. Then, for $\varsigma > 0$ k_{eff} (shape) increases promptly and rapidly. Already for a non-coverage of $\varsigma = 5\,\text{cm}$ a significant increase of k_{eff} (shape), compared to the values obtained for k_{eff} (shape) at $\varsigma \leq 0$, is found. So therefore, it has to be considered that cases as those described in the first paragraph of this section result in significant impacts on k_{eff} (shape). In other words, one has to be very cautious when choosing the nominal length of absorber channels equal to the nominal active length specified for the unirradiated fuel assemblies.

If this choice is made for a burnup credit transport cask it has to be taken into account that the non-coverage of the fuel zone of the fuel assemblies may be increased due to slipping of the fuel assemblies under accident conditions which results, if flooding of the cask is assumed to be caused by these accident conditions, in a significant increase of k_{eff} (shape), cf. Figure 22. And it should be kept in mind that the increase of k_{eff} (shape)

- takes place the prompter the higher the average burnup of the axial burnup profiles is, and
- is significantly enhanced if CR insertion during depletion of the fuel assemblies has to be considered.

In conclusion, it is strongly recommended to ensure full coverage of the fuel zones under all conditions to be analyzed in a burnup credit application case.

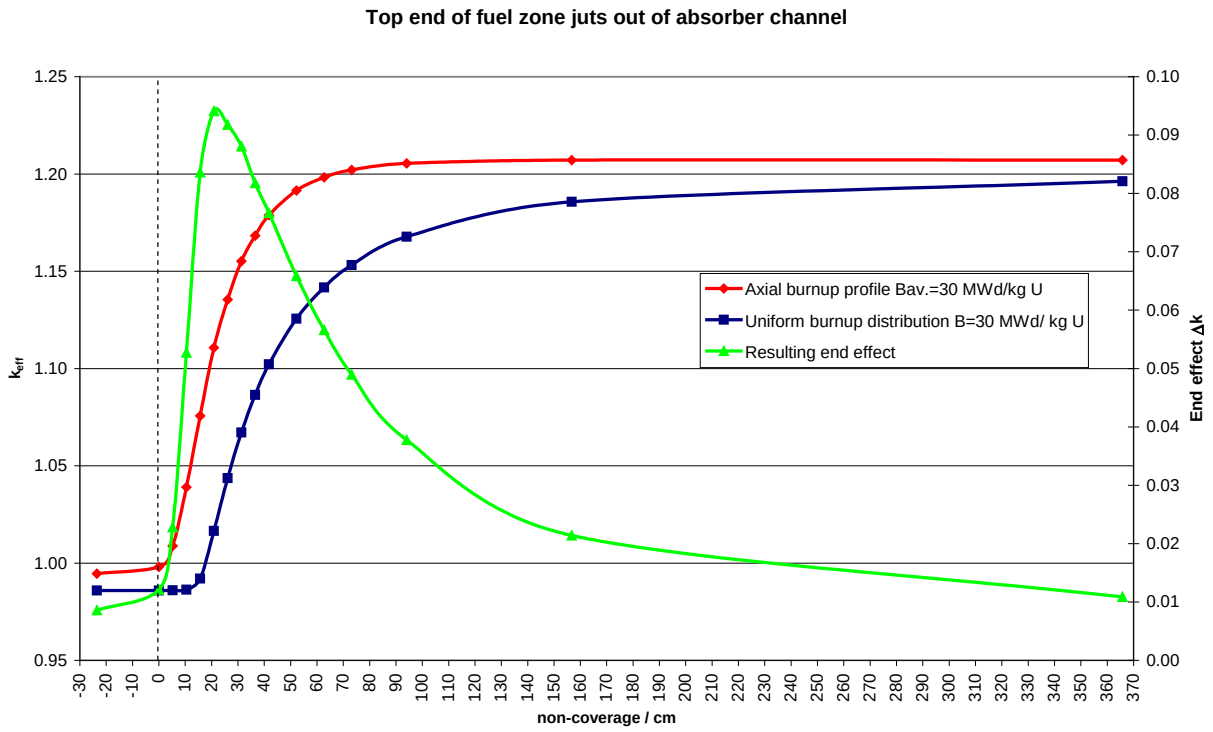

Figure 22

5 Conclusions

It has been shown that it is possible to predict qualitatively, on the basis of the results obtained in the Phase II-C benchmark, the behavior of k_{eff} (shape), k_{eff} (unif. dist.) and hence the end effect for the Phase II-E configurations as well as for the case that the fuel zone of spent fuel assemblies is not fully shielded by neutron absorbing channels. The lessons learnt from elaborating these predictions and from the results obtained for the Phase II-E configurations and the case of partial non-coverage of the fuel zones are as set forth below:

- In generell, the reactivity behavior of spent PWR UO_2 fuel differs from the reactivity behavior of unirradiated fuel PWR UO_2 (E.g., in case of partial non-coverage of the fuel zones the reactivity behavior of spent fuel cannot be derived from the reactivity behavior of unirradiated fuel, cf. section 4).
- The end effect strongly depends on
  - the depletion conditions, (in particular, on the CR insertion history during irradiation),
  - the asymmetry and "local asymmetry" of the axial burnup profile (catchword: "bounding profile", [5]) chosen to analyze the end effect, and
  - the design of the spent fuel management system of interest.
- The end effect has to be controlled. If the end effect is negative the uniform burnup of the average burnup of the analyzed axial burnup profile is the bounding profile.

The lessons learnt from elaborating the predictions made and from the results obtained for Phase II-C through Phase II-E and the case of partial non-coverage of the fuel zones help to avoid errors in the design of devices, systems or installations for handling, transport or storage of spent PWR UO_2 fuel assemblies. It is strongly recommended, for instance, to ensure full coverage of the fuel zones under all conditions to be analyzed in a burnup credit application case.

References

[1] M. Takano and H. Okuno, "OECD/NEA Burn-up Credit Criticality Benchmark: Results of Phase II-A", Report Jaeri-Research 96-003, NEA/NSC/DOC(96)01, February 96

[2] A. Nouri, "OECD/NEA Burnup Credit Criticality Benchmark, Analysis of Phase II-B Results: Conceptual PWR Spent Fuel Transportation Cask", IPSN / Département de Prévention et d'Etude des Accidents / Service d'Etudes de Criticité Rapport IPSN/95-05, NEA/NSC/DOC(98)1

[3] Jens Christian Neuber, "Burn-up Credit Criticality Benchmark, Phase II-C, Impact of the Asymmetry of PWR Axial Burn-up Profiles on the End Effect", OECD 2008, NEA N°. 5435, ISBN 978-92-64-99049-4

[4] Annme Barreau, "Burn-up Credit Criticality Benchmark Phase II-D, PWR UO2 Assembly, Study of control effects on spent fuel composition", OECD 2006, NEA No. 6227, ISBN 92-64-02316-X

[5] Jens-Christian Neuber, "Generation of Bounding Axial Burnup Profiles as a Continuous Function of Average Burnup", Proceedings of the 7th International Conference on Nuclear Criticality Safety ICNC 2003 (JAERI-Conf 2003-19), pp 672-677

[6] Thomas Lamprecht, Gemeinschaftskraftwerk Neckar GmbH; Nuclear Power Plant Neckar-westheim II, "GKN II: Axial Burnup Profiles from Fuel Assemblies with Zircaloy Spacer Grids", data file ABBRDAT.ZIP send by e-mail dated May 05, 2000

[7] Jens Christian Neuber and Michael Schmid, Paul Bryce and Alwin Wiederhold, "Selection and Evaluation of Bounding Depletion Conditions and Axial Burn-Up Profiles for a Burn-Up Credit Criticality Safety Analysis of the Sizewell B Wet Storage Pond", Proceedings of the 8th International Conference on Nuclear Criticality Safety ICNC 2007 St. Petersburg Russia, Vol. II pp. 117-123

[8] Jens Christian Neuber, "Specification for Phase II-E Benchmark:", http://www.nea.fr/html/science/wpncs/buc/specifications/index.html

[9] J.C. Neuber, "Calculation routes to determine burnup credit loading curves", Proceedings of the IAEA TM 2005 on "Advances in Applications of Burnup Credit to Enhance Spent Fuel Transportation, Storage, Reprocessing and Disposition", IAEA-TECDOC-1547, pp. 271-286